Infrared Multiple Photon Dissociation Spectra of Cesiated Complexes of the Aliphatic Amino Acids: Challenges for Conformational-Space Calculations by Density Functional Theory

P. B. Armentrout,*[,†] Ryan P. Steele,[†] Brandon C. Stevenson,[†] Roland M. Jones,[†] Jonathan Martens,[‡] Giel Berden,[‡] and Jos Oomens[‡,§]

[†]Department of Chemistry, University of Utah, 315 South 1400 East Room 2020, Salt Lake City, Utah 84112, United States

[‡] Radboud University, Institute for Molecules and Materials, FELIX Laboratory, Toernooiveld 7, NL-6525 ED Nijmegen, The Netherlands

[§]Van't Hoff Institute for Molecular Sciences, University of Amsterdam, Science Park 904, Amsterdam, The Netherlands

Abstract: Cesiated complexes of the aliphatic amino acids (Gly, Ala, hAla, Val, Leu, and Ile) were examined by infrared multiple photon dissociation (IRMPD) action spectroscopy utilizing light from a free-electron laser (FEL). To identify structures, the experimental spectra were compared to linear spectra calculated at the B3LYP-GD3BJ/def2-TZVP level of theory. Relative energies at 0 and 298 K for various possible conformers of all complexes were calculated at B3LYP, B3LYP-GD3BJ, and MP2(full) levels using the def2-TZVP basis set. Spectral comparison for all complexes indicates that the dominant conformation has the cesium cation binding to the carbonyl and hydroxyl oxygens, [CO,OH]. This conclusion contrasts with previous work for Cs^+(Gly), which suggested that the [CO] binding motif was prevalent. This dichotomy is explored theoretically in detail using coupled-cluster calculations with single, double, and perturbative triple excitations, CCSD(T), as well as advanced density functional theory (DFT) approaches. The comparisons show that the [CO,OH] – [CO] double-well potential found for most DFT approaches disappears at the higher level of theory with only the [CO,OH] well remaining. An exploration of this effect indicates that electron correlation is critically important and that DFT approaches incorrectly handle the internal hydrogen bonding in these molecules, thereby over-delocalizing the charges on the amino acid ligands.

INTRODUCTION

Gal et al. have reviewed the binding affinities of the cesium cation to various molecules and established the interest in such studies.[1] Atmospheric testing of thermonuclear devices and nuclear reactor accidents have both introduced radioactive cesium isotopes into the environment. Their interactions with biological systems have health consequences because Cs^+ is known to follow the same biological pathways and bind at the same sites as K^+,[2, 3] an essential nutrient. Nevertheless, the transport and accumulation rates of cesium cations differ from those of potassium cations,[4-7] allowing them to be used as agents in imaging of tissue and tumors.[8]

Previously, we have used threshold collision-induced dissociation (TCID) in a guided ion beam tandem mass spectrometer to measure the interactions of cesium cations with many amino acids (AA): glycine (Gly), proline (Pro), serine (Ser), threonine (Thr), cysteine (Cys),[9] methionine (Met), phenylalanine (Phe), tyrosine (Tyr), tryptophan (Trp),[10] aspartic acid (Asp), asparagine (Asn), glutamic acid (Glu), glutamine (Gln),[11] and histidine (His).[12] Analysis of these data provides absolute bond dissociation energies (BDEs) for the Cs^+(AA) interactions, which can be favorably compared with theoretical values predicted for the lowest-energy conformations. In some cases, however, different levels of theory identify different structures as the lowest-energy complex. To resolve such ambiguities, we have also performed studies of these complexes using infrared multiple photon dissociation (IRMPD) action spectroscopy because the IR spectrum of the complex is a more sensitive probe of the structures than the BDE.

IRMPD studies of the entire sequence of alkali metal cations (Li^+, Na^+, K^+, Rb^+, Cs^+) have been conducted for M^+(Pro),[13] M^+(N-methyl Ala),[13] M^+(Ser),[14] M^+(Thr),[15] M^+(Cys),[16] M^+(Met),[17] M^+(Asn),[18] M^+(His),[19] and most recently, M^+(Gly).[20] Sodiated Gly and Pro as well as lithiated and cesiated Asp and Glu have also been examined.[21, 22] In general, these studies find that the smallest cations, Li^+ and Na^+, bind to the amino nitrogen and carbonyl oxygen, denoted as [N,CO] here, augmented by complexation to a functionalized side chain when available. Spectra for the three heavier alkali cations are generally more complicated, showing evidence for these same isomers, as well as an increasing preference for binding to the two oxygens

of the carboxylic acid, either [CO,OH] or [CO_2^-] if the AA is zwitterionic. In the M^+(Gly) study, discrepancies among different levels of theory were particularly problematic for the heavier alkali cations because some levels of theory indicated that a [CO] isomer, in which the metal ion interacted only with the carbonyl oxygen, was the lowest-energy structure. Notably, these three structures are all directly coupled to one another, i.e., a double-well potential exists between the [CO] and [CO,OH] complexes, and the latter structure couples via a double-well potential to the [CO_2^-] zwitterionic form. Because of this ambiguity, several levels of theory were explored, and we concluded that the [CO] structure was probably favored.

From a broader perspective, the computational ambiguity in locating the most stable structure is highly problematic. If computational methods cannot reliably predict the lowest-energy isomer for the simple metallated aliphatic amino acids, where the binding modes are limited, then predictions for amino acids with functionalized side chains are also in doubt, as are theoretical results for peptides, proteins, and more complicated biological systems. Therefore, we initiated the present study to examine the IRMPD spectrum of the cesiated aliphatic amino acid complexes: alanine (Ala), homo-alanine (hAla), valine (Val), leucine (Leu), and isoleucine (Ile). In the work presented here, we revisit the Cs^+(Gly) complex using higher levels of theory and explore the influence of the side-chain. For the longer side-chains, their conformational flexibility allows multiple low-energy conformations to be formed,[23] which are explored in some detail. For all complexes, quantum chemical calculations at several levels of theory are carried out to provide structures and vibrational frequencies needed for comparison to the IRMPD data.

EXPERIMENTAL AND THEORETICAL METHODS

Mass Spectrometry and Photodissociation

Experiments were performed at the Free-Electron Lasers for Infrared eXperiments (FELIX) Laboratory at Radboud University in the Netherlands.[24] IRMPD spectra were acquired using the FELIX beamline and a quadrupole ion trap (QIT) mass spectrometer (Bruker, Amazon Speed ETD) modified to allow optical access.[25] Ions were generated by electrospray ionization

from solutions containing ~10 μM amino acid and cesium chloride salt (obtained from commercial sources and used without any further purification) in a 1:1 methanol-water mixture. Metallated complexes were mass isolated and irradiated with a single macropulse from the free-electron laser at a repetition rate of either 10 Hz with powers up to 150 mJ per pulse and a bandwidth of ~0.5% of the central frequency. Infrared action spectra were generated by plotting the photofragmentation yield (Y) as a function of the laser frequency using the equation $Y = -\ln[\Sigma I_P / (\Sigma I_F + \Sigma I_P)]$, where the I_P (precursor) and I_F (fragment) ion mass peaks are the integrated intensities.[26] In all cases, the Cs^+(AA) complexes dissociated to form Cs^+. To account for frequency-dependent variations in the FEL power, a linear correction was applied to the yield.[26, 27] This power correction is appropriate because the dependence on power is nearly linear because the multiple photon excitation process is incoherent rather than coherent, at least until saturation begins.

Computational Details

Most computations needed in the present study utilized the Gaussian 16 suite of programs[28] to calculate vibrational frequencies and structures of the cesiated complexes of interest. Geometries for these complexes were initially optimized at the B3LYP/def2-TZVP level.[29-31] The def2-TZVP basis set is a size-consistent triple-ζ basis set with polarization functions and a small-core (46 electrons) effective core potential (ECP) on Cs^+. Geometry optimizations of metalated structures were also conducted including corrections for empirical dispersion at the B3LYP-GD3BJ[32, 33] and at the MP2(full)[34] (where full refers to the correlation of all electrons beyond the ECP, abbreviated as MP2 below) levels using the same basis set. The def2-TZVP basis set and corresponding ECP were obtained from the basis set exchange website.[35]

Vibrational frequencies were scaled for comparison to the IRMPD spectra, because a scaling factor is needed to account for known inaccuracies in the calculated harmonic frequencies, giving generally good agreement with well-resolved peaks in other IRMPD spectra. In the present system, the scaling factor was adjusted as described below. The calculated frequencies were broadened using a 40-cm^{-1} full-width-at-half-maximum Gaussian line shape when used for

comparison to the experimentally determined spectra. The broadening accounts for the finite laser bandwidth, unresolved rotational envelope, anharmonic broadening of the vibrational bands, and broadening resulting from the multiple-photon absorption process.

Single-point energy calculations were carried out for the most stable structures at the B3LYP//B3LYP, B3LYP-GD3BJ//B3LYP-GD3BJ, and MP2//MP2 levels of theory using the def2-TZVPPD basis set. Zero–point vibrational energy (ZPE) and thermal corrections were determined using vibrational frequencies calculated at the B3LYP/def2-TZVP level after scaling by a factor of 0.989 to account for known inaccuracies.[36, 37] ZPE corrections were applied to single-point energies in order to provide 0 K relative enthalpies. Thermal corrections to obtain 298 K Gibbs energies were calculated from 0 K relative enthalpies by using the rigid rotor/harmonic oscillator approximation with the calculated rotational constants and vibrational frequencies.

In order to more thoroughly assess the computational methodology dependence, we also performed calculations for the Cs^+(Gly) complex at several additional levels of theory, including coupled-cluster with single and double excitations (CCSD)[38] and added perturbative triple excitations [CCSD(T)].[39] The SCAN0[40] and range-separated hybrid ωB97M-V[41] functionals were employed to investigate the roles of functional properties. The correlation-consistent, triple-ζ cc-pwCVTZ-PP basis set[42] was used for Cs, along with the ECP46MDF pseudopotential;[43] the valence and all sub-valance electrons were correlated in the wavefunction-based correlated calculations. The cc-pVTZ basis set[44] was used for the {C,N,O,H} atoms, and the frozen-core approximation was employed for these atoms in correlated calculations.

RESULTS AND DISCUSSION

Nomenclature

Structures of the Cs^+(AA) complexes are designated by specifying metal binding sites in square brackets, followed by the amino acid dihedral angle orientation, as outlined in Figure 1. Metal binding sites are identified as the amino nitrogen (N), carbonyl oxygen (CO), hydroxy group

(OH), or both oxygens of a carboxylate group (CO_2^-). The ∠HOCC$^\alpha$ and ∠OCC$^\alpha$N dihedral angles are characterized as c (cis) for angles <50°, t (trans) for those >135°, and g (gauche) for all intermediate angles. For the four amino acids having a side chain longer than Ala, this designation is followed by a description of the side chain dihedral angle orientations in parentheses as ∠CC$^\alpha$C$^\beta$C$^\gamma$ for homoalanine, ∠CC$^\alpha$C$^\beta$H for valine, ∠CC$^\alpha$C$^\beta$C$^\gamma$ and ∠C$^\alpha$C$^\beta$C$^\gamma$H for leucine, and ∠CC$^\alpha$C$^\beta$C$^\gamma$ and ∠C$^\alpha$C$^\beta$C$^\gamma$C$^\delta$ for isoleucine. In order to distinguish between otherwise-identical names, + and − subscripts may also be given for some gauche angles. As shown in Figure 1, there is one nuance to the [N,CO]-tt structures for all complexes except Gly; namely, the cesium cation can tilt towards or away from the side chain (R), which we designate as S for syn or A for anti, respectively.

IRMPD Action Spectroscopy: Comparison

IRMPD action spectra for the cesiated complexes of AA = Gly, Ala, hAla, Val, Leu, and Ile were acquired from 5.2 to 17 μm (580−1850 cm^{-1}), as shown in Figure 2. Photodissociation of all complexes resulted in a loss of the intact AA to form Cs^+ as the only ionic fragment. All of the spectra share many common features and a few distinct differences. The most intense peak is found at 1745 cm^{-1} for Cs^+(Gly) but redshifts to 1740 (Ala), 1726 (hAla), 1733 (Val), 1730 (Leu), and 1728 (Ile) cm^{-1} for the heavier AAs. The second most intense peak is found near 1370 cm^{-1}, sometimes with a small shoulder near 1470 cm^{-1}. All spectra exhibit a pair or triad of peaks ranging from 800 – 1000 cm^{-1} and there is also a very weak band located near 1170 cm^{-1}. Clearly, the structures of all complexes are probably similar.

Cs^+(Gly): Theoretical Results

In our previous exploration of the Cs^+(Gly) system,[20] one of the interesting observations was the dichotomy of theoretical results for the lowest-energy structure where Cs^+ binds to the carbonyl oxygen. The dipole moment of the CO favors putting the cation directly along the CO bond (CsOC bond angle of 180°) in a [CO]-cc structure; however, additional binding to the

hydroxyl oxygen provides a bidentate interaction, [CO,OH]-cc, Figure 1. We found that B3LYP calculations favored the [CO]-cc structure whereas MP2 calculations found a [CO,OH]-cc ground structure. Including empirical dispersion (GD3BJ) yielded both structures with [CO]-cc slightly lower in energy. To evaluate these disparate results from a theoretical point of view, here we have examined the potential energy surface (PES) for interconversion between these structures at additional levels of theory using the cc-pwCVTZ-PP basis set. The results are shown in Figure 3. As before, B3LYP strongly favors the [CO]-cc structure, and the [CO,OH]-cc structure is not a local minimum but an inflection point along the PES. Again, adding dispersion (GD3BJ) leads to local minima for both structures with [CO]-cc favored. The SCAN0 functional yields very similar results. The range-separated ωB97M-V hybrid functional retains the two minima, but now the [CO,OH]-cc structure is favored. As before, MP2 calculations strongly favor the [CO,OH]-cc bidentate species, and the [CO]-cc structure is only an inflection point along the PES. Finally, the CCSD(T) results, which serve as reference calculations in the present analysis, follow the MP2 PES fairly closely, although the [CO]-cc structure is stabilized slightly. Clearly, the DFT approaches do not adequately account for the Cs^+-OH interaction. Although the range-separated hybrid functional comes closest to the CCSD(T) results, it still finds a potential well for the [CO] structure. Given that the MP2, CCSD, and CCSD(T) methods all agree on the absence of this secondary minimum, we suspect that its existence is an artifact of the density functionals examined here.

As discussed in our previous work,[20] the implications that this distorted PES has on the observed species is interesting. We pointed out that the potentials shown do not include zero-point energies (ZPE) nor enthalpic and entropic thermal corrections. In our previous work, which used B3LYP/def2-TZVP calculations for [CO]-cc and MP2/def2-TZVP calculations for [CO,OH]-cc, the ZPE for the [CO,OH]-cc structure was larger than that for [CO]-cc by 1.7 kJ/mol and a 298 K thermal correction (including ZPE) to give ΔG_{298} was 4.4 kJ/mol. Here, we use a more balanced approach by using B3LYP-GD3BJ/def2-TZVP calculations for both species. This leads to the ZPE for [CO,OH]-cc being *smaller* than that for [CO]-cc by 0.2 kJ/mol and 0.3 kJ/mol larger at 298 K

(energies well within any theoretical uncertainty). The entropic correction at 298 K favors the monodentate [CO]-cc structure because the metal ion can move more freely than in the bidentate [CO,OH]-cc. If these energies are included in the potentials shown in Figure 3, the overall PES retains the same basic shape. Previously, we concluded that the system could spend more time in the entropically favored [CO]-cc structure whether the surface looks like those calculated with the DFT or the CCSD(T) methods. This conclusion was consistent with our comparison between the experimental and theoretical spectra, which led us to conclude that the observed spectrum was most consistent with the [CO]-cc structure, although contributions from the [CO,OH]-cc structure could not be eliminated. We now revisit that conclusion here.

Cs^+(Gly): Comparison of Experimental and Theoretical Spectra

We have previously published an IRMPD spectrum for Cs^+(Gly) recorded using a Fourier transform ion cyclotron resonance (FTICR) mass spectrometer.[20] As shown in the Supporting Information in that work, the present spectrum taken on the ion trap instrument reproduces most of the bands except a prominent one in the FTICR spectrum at 1599 cm^{-1} is found around 1577 cm^{-1} with much weaker intensity in the ion trap. In the ion trap, which has a higher background pressure than the FTICR, such weak bands can lose intensity because collisional deactivation removes energy on the same time scale as the photoexcitation.[45, 46] For a strongly anharmonic band, such as this one,[13-19, 22, 47-57] this can also shift the position of the band as a result of anharmonicities coupled with multiple photon effects. Further, the bands between 800 and 1000 cm^{-1} are better resolved in the ion trap spectrum used here, Figure 2. Our previous work established that the spectrum was generally consistent with the [CO]-cc and [CO,OH]-cc structures and not with alternative structures (including [CO_2^-]), all of which are much higher in energy according to all levels of theory explored. A key aspect of these comparisons was that calculations for the [CO]-cc structure were performed at the B3LYP/def2-TZVP level because the MP2 calculations collapsed to [CO,OH]-cc. In contrast, calculations for [CO,OH]-cc utilized the MP2/def2-TZVP level of theory because the B3LYP approach collapsed to [CO]-cc. Anharmonic calculations were

also performed for both conformers and, although many bands shifted somewhat, the overall anharmonic spectrum showed little difference from the scaled harmonic spectrum in the frequency range studied (see Figure 9 of ref. [20]), with the only exception being a red-shift in the minor band near 1620 cm^{-1} in the harmonic spectra (identified as an NH_2 scissors motion) to 1600 cm^{-1} in the anharmonic spectrum. From these comparisons, we concluded that the [CO]-cc structure was most consistent with the experimental spectrum, largely because the band at 1745 cm^{-1} was reproduced slightly better by the scaled [CO]-cc spectrum and the [CO,OH]-cc structure had a predicted band at about 1000 cm^{-1} that was not observed.

Here, we take a more balanced approach and utilize harmonic spectra calculated at the B3LYP-GD3BJ/def2-TZVP level, which exhibits a well for both the [CO]-cc and [CO,OH]-cc species, Figure 3. Thus, the two spectra can be compared more directly and fairly. We also avoid using a universal scaling factor (0.975 in the previous work) and instead scale the spectra so that the sharp band at 1745 cm^{-1} (which corresponds to the C=O stretch coupled with in-plane COH bend) is best reproduced. This approach leads to a scaling factor of 0.98 for [CO]-cc and 0.97 for [CO,OH]-cc. The comparison with the experimental spectrum is shown in Figure 4a. This comparison makes it clear that the distinction between the two spectra is minimal, although the intensity of the C=O stretch is higher by about 100 km/mol in the [CO]-cc spectrum. The band near 1400 cm^{-1} is now predicted at 1387 cm^{-1} for [CO,OH]-cc and at 1411 cm^{-1} for [CO]-cc, where the former agrees better compared to the peak in the experimental spectrum at 1368 cm^{-1}. The minor band near 1200 cm^{-1} also shifts, from 1190 cm^{-1} for [CO,OH]-cc to 1226 cm^{-1} for [CO]-cc, such that the former again agrees better compared to 1176 cm^{-1} in the experiment. Both of these bands correspond to in-plane COH bends with different phase relationships with the adjacent C-O stretch. The two bands predicted at 889 and 814 cm^{-1} for [CO,OH]-cc and 896 and 818 cm^{-1} for [CO]-cc are both NH_2 wags. These transitions both match the experimental peaks at 884 and 812 cm^{-1} well. In general, the [CO,OH]-cc spectrum agrees slightly better with experiment especially with regard to reproducing the experimental bands at 1368 and 1176 cm^{-1}. For both predicted

spectra, the main difference with experiment is the failure to observe the band predicted near 950 cm^{-1}.

At this point, a reviewer raised an interesting point: although use of a scaling factor is commonly applied because of its statistical improvement to computed spectra, the more detailed examination being conducted here could potentially be flawed because the anharmonic character of individual vibrational modes could be non-uniform. As noted above, we previously found that the scaled harmonic and anharmonic spectra were similar except for one strongly anharmonic band. Here, we check this attribute by performing anharmonic calculations for both the [CO,OH]cc and [CO]-cc complexes calculated using the B3LYP-GD3BJ approach. The resulting spectra are compared to experimental results in Figure S1 of the Supporting Information. In the range of 600 – 1900 cm^{-1}, none of the bands of either conformer show a very large anharmonicity shift, essentially confirming that use of a uniform scaling factor is appropriate in this range. For the [CO,OH]-cc geometry, the most anharmonic vibration is the one previously identified, the NH_2 scissors near 1575 cm^{-1}. As before, the anharmonic spectra are similar to the scaled harmonic spectra except the bands near 1400 cm^{-1} are broader (but the relative positions remain the same as Figure 3) and the out-of-plane OH wags near 950 cm^{-1} have red-shifted to near 927 cm^{-1} and are lower in intensity. A more quantitative comparison of the unscaled anharmonic spectra with experiment (eight bands) shows that the average deviation between experiment and the calculation is 0.1 ± 7.9 cm^{-1} for the [CO,OH]-cc geometry and 9.0 ± 20.4 cm^{-1} for the [CO]-cc structure. (Mean absolute deviations are 7 ± 4 and 15 ± 16 cm^{-1}, respectively.) Further, the experimental difference between the two major bands at 1745 and 1368 cm^{-1} of 377 cm^{-1} is predicted to be 378 cm^{-1} for [CO,OH]-cc and 356 cm^{-1} for [CO]-cc. By any measure, the [CO,OH]-cc spectrum agrees slightly better with experiment than that for [CO]-cc, in agreement with the conclusion from the scaled harmonic spectra.

The conclusion that the [CO,OH]-cc spectrum is a slightly better match to the experimental spectrum contrasts with the opposite conclusion reached earlier.[20] As noted above, the previous conclusion was based on two main observations. 1) The band at 1745 cm^{-1} was matched better by

the B3LYP [CO]-cc spectrum compared to the MP2 [CO,OH]-cc spectrum when both theoretical spectra were scaled by 0.975. Here, if we scaled the MP2 [CO,OH]-cc spectrum to match this band, a scaling factor of 0.96 is needed. This scaled spectrum matches that shown in Figure 4a for the B3LYP-GD3BJ spectrum except the 950 cm^{-1} band in the B3LYP-GD3BJ spectrum (an out-of-plane OH wag) has shifted to 991 cm^{-1}. 2) The failure to observe this 991 cm^{-1} band was the other reason that we favored the [CO]-cc structure. The comparison here shows that the DFT-based approaches shift this band to a lower frequency (and thus closer to the experimental band), but this observation is true for both the [CO]-cc and [CO,OH]-cc structures, such that the lack of this band no longer favors one structure over the other. The sharper experimental spectrum used here for comparison strongly suggests that this band is not observed in contrast to the B3LYP, B3LYP-GD3BJ, and MP2 predictions.

To aid in resolving this discrepancy, the CCSD spectrum of [CO,OH]-cc was computed for comparison to experiment, as shown in Figure 4b. When scaled by 0.94, this spectrum is very similar to those of the B3LYP-GD3BJ and MP2 spectra, except the 991-cm^{-1} (MP2) and 950-cm^{-1} (B3LYP-GD3BJ) band has shifted here to 902 cm^{-1}. The CCSD spectrum has major peaks at 1748, 1589, 1381, 902, 895, and 815 cm^{-1}, which compare well with the experimental peaks at 1745, 1575 (1600, FTICR spectrum), 1368, 884, and 812 cm^{-1}. Because the band previously predicted at 991 or 950 cm^{-1} has shifted to 902 cm^{-1}, where it overlaps with the predicted 895 cm^{-1} band, the CCSD spectrum reproduces the experimental spectrum (which has no band at 950 or 991 cm^{-1}) better than the B3LYP-GD3BJ or MP2 spectra. Figure 4b also shows that several minor bands predicted at the CCSD level are also found experimentally, although relative intensities can vary. These include predicted bands at 627 (in-plane OCO and NCC bends), 1040 (CN stretch), and 1193 cm^{-1} (CO stretch and in-plane COH bend) compared to experimental bands at 641, 1059, and 1176 cm^{-1}.

Origins of the challenges to DFT

The coupled-cluster results presented herein provide an internal reference for the assessment of more computationally economical methods, such as MP2 and DFT. For larger biological complexes, however, coupled-cluster computations quickly become impractical, and the latter alternative methods are currently necessary. The source of the poor performance of the density functionals, therefore, warrants additional investigation.

In particular, we sought to determine the source of the differences in relative energies between [CO]-cc and [CO,OH]-cc structures calculated using DFT-based and wavefunction-based electron-correlation methods. We note from the outset that these discrepancies are subtle effects, comprising shifts of ≈4 kJ/mol at most. Nonetheless, these same differences dictate qualitative changes in the binding orientation of the ion and, accordingly, the corresponding vibrational spectra.

Energies. Similar to Figure 3, Figure S2 in the Supporting Information shows the relative energies along a C-O_{OH}-Cs^+ coordinate. Figure S2 adds CCSD and HF results to the analysis and omits SCAN0 and B3LYP-GD3BJ results. As in Figure 3, the reference CCSD(T) method exhibits a single minimum at the bidentate [CO,OH]-cc structure and only a slight inflection near the [CO]-cc structure. Like the MP2 approach, the CCSD method is qualitatively similar to CCSD(T), although the energy of the [CO]-cc inflection point is method-dependent. The HF method erroneously predicts only a single [CO]-cc minimum and shows almost no inflection near the [CO,OH]-cc minimum; evidently the existence of the latter minimum depends strongly on electron-correlation effects. This factor likely explains the relative (albeit incomplete) improvement to B3LYP by empirical dispersion terms, Figure 3. As shown in Figure 3, the hybrid B3LYP functional provides some degree of stabilization in the [CO,OH]-cc region, but otherwise performs closer to the HF limit. As shown in both Figures 3 and S1, the range-separated ωB97M-V functional properly predicts a deeper [CO,OH]-cc well, although a shallow, spurious [CO]-cc minimum remains, as discussed above.

Energy Components. Under the hypothesis that known DFT charge-transfer pathologies could perhaps be responsible for the DFT behavior, an energy-decomposition analysis[58] (EDA)

was performed for the HF, B3LYP, and ωB97M-V methods. Using Cs^+ and Gly as two distinct fragments, with [CO,OH]-cc and [CO]-cc structures (shown in Figure S2), Figure S3 presents the EDA interaction-energy components for three main categories. The first component is the electrostatic ("frozen") interaction between the two fragments, during which the interaction between fixed charge densities of the two fragments is computed. This component is the strongest of the three computed components, which could be expected for an ion-containing complex. Less obvious is the fact that the better-performing ωB97M-V functional exhibits qualitatively different behavior near the [CO,OH]-cc structure. Unlike HF and B3LYP, the electrostatic component exhibits a preference for this structure with the ωB97M-V method.

The remaining two EDA components describe the mutual response of fragment electron densities. The polarization term quantifies the energy lowering from relaxation of the fragment electrons *without* allowing charge transfer to take place. Although HF and the density functionals differ in their relative behavior across the angle scan, the two density functionals nearly parallel one another across the range of angles examined. Therefore, polarization does not distinguish the behavior of the two functionals. Finally, the delocalization term accounts for charge-transfer effects between the fragments and any higher-order relaxation effects. This term was the original focus of our analysis, as it would suggest the degree to which DFT was (over-)delocalizing the charge between fragments. Indeed, the degree of charge transfer is notably larger in the density functionals than in HF, and B3LYP exhibits larger charge transfer than in ωB97M-V. Nevertheless, the two functionals again nearly parallel one another and provide little insight into the differing total interaction-energy behavior. Thus, the electrostatic interaction evidently stands alone as the sole arbiter of the discrepancy between methods.

Partial Charges. Given the dominant electrostatic contribution, we further investigated the charge distributions along the same angle scan. Unlike the EDA analysis, MP2 results can be included in this investigation (all MP2 charges were computed from properly relaxed electron densities amidst an MP2 force calculation). Charges for Cs, O_{OH}, and O_{CO} are depicted in Figure S4.

The Cs charge (which ranges from +0.89 to +0.94) differs between methods, which is consistent with the differing charge-transfer energies in Figure S3; however, the Cs charge varies similarly across methods. The O_{CO} charge exhibits a similar lack of variation between methods, although the set of correlated methods exhibits a notably smaller overall magnitude than HF. More nuanced behavior is observed in the O_{OH} charge. Between 65° and 90° (the transition region between stable structures), the ωB97M-V charge essentially transforms from the B3LYP charge near the [CO]-cc minimum to the MP2 charge near the [CO,OH]-cc minimum. This behavior, in particular, is consistent with the ωB97M-V method predicting both a stable [CO,OH]-cc minimum and some degree of spurious [CO]-cc stabilization. Therefore, the absolute magnitudes of the charges are reflective of differences between methods, but only the O_{OH} charge suggests a difference in behavior between the two minima.

On the basis of the electrostatic components of the EDA results, we surmised that the charge distribution within the Gly monomer could be responsible for at least some of the differences between functionals. The Charges from the Electrostatic Potential on a Grid ("ChElPG") partial charges for both the complex and the isolated Gly molecule (with the latter optimized for each method) are presented in Table S1. These charges demonstrate two qualitative outcomes that account for the difference in methods:

(a) The partial charge on the O_{CO} atom is smaller in magnitude with MP2 than with either density functional. This trend is consistent in *both* the complex and the Gly molecule.

(b) The hydrogen-bonded -OH···NH_2 unit within the Gly molecule exhibits more charge delocalization with the DFT methods. The MP2 method exhibits more charge separation—and, importantly, a larger O_{OH} charge—than the functionals. This behavior is consistent with the propensity of DFT to over-emphasize hydrogen-bonding effects.

Therefore, the density functionals exhibit larger O_{CO} charges (likely a result of electron correlation) and smaller O_{OH} charges (resulting from charge delocalization within the H-bonded moiety). Both of these properties are consistent with the overall ion-position relative energies. Furthermore, the O_{OH} charge from ωB97M-V exhibits closer fidelity to the MP2 charge than

B3LYP does, which is also consistent with better [CO,OH]-cc stabilization with ωB97M-V. The overestimation of the charge on O_{CO} was observed to occur *even within the isolated Gly monomer*, suggesting that charge delocalization across the ion-molecule complex is not the sole arbiter of this effect.

Note also that the large change in the intramolecular -OH···NH_2 hydrogen-bond explains why the vibrational frequency observed to shift most severely between the DFT and CCSD spectra is the out-of-plane OH wag. To explore the consequences of this effect further, we examined the high-frequency region of the vibrational spectrum (Figure S5). This comparison shows that the density functionals red-shift the hydroxy O-H stretching mode—the bright transition in this region—by an appreciable amount (130 – 160 cm^{-1}), compared to the CCSD reference spectrum, although this effect is somewhat tempered by the ωB97M-V functional. The HF spectrum is even further shifted, now to the blue, because of the lack of electron correlation. These spectral signatures are consistent with the charge analysis of Figure S4 and Table S1.

Figure S6 compares the CCSD spectrum for the [CO,OH]-cc structure scaled by 0.955[59] to the experimental spectrum taken over a range of 1900 – 3400 cm^{-1}. The spectrum is extremely broad although one sharp peak at 2962 cm^{-1} was also observed. The latter peak corresponds to the predicted band at 2963 cm^{-1}, the symmetric CH stretch of the CH_2 group. The broad band is consistent with a strongly hydrogen bonding OH stretch,[60] predicted to occur at 3244 cm^{-1}. The breadth of this band is sufficiently large that the red-shifted bands in the DFT spectra (now near 3100 cm^{-1}) are still potentially consistent with observation. Finally, predicted bands associated with the symmetric and asymmetric NH stretches of the NH_2 group at 3414 and 3488 cm^{-1} are slightly above the experimental range. Overall, the spectrum demonstrates that the OH stretch is severely broadened, consistent with strong hydrogen bonding in Cs^+(Gly).

Cs^+(AA): Theoretical Results

As the complexity of the side chain increases, theoretical results increasingly favor the [CO,OH]-cc structure. This is shown by the PESs for Cs^+(Ala) and Cs^+(Val) in Figure 5. Neither

B3LYP nor B3LYP-GD3BJ calculations have a local minimum for the [CO]-cc species and the MP2 well becomes much more harmonic-like. The increasing size (and polarizability) of the side chain presumably has an inductive effect that donates electron density to the carboxylic acid group, making the bidentate coordination increasingly more favorable. We conclude that, as for the case of Cs^+(Gly), we can utilize the [CO,OH]-cc results for these larger aliphatic amino acids.

As the side chain increases in length, multiple conformers of the [CO,OH]-cc structure evolve for hAla, Val, Leu, and Ile. We explored these in some detail for the case of K^+(AA).[23] Calculations of the relative 0 K enthalpies and 298 K Gibbs energies for these variants of the cesiated complexes are included in Table 2. These results indicate that there is a dominant conformation for Cs^+(Val) ([CO,OH]cc(g_+)), Cs^+(Leu) ([CO,OH]cc(tg_+)), and Cs^+(Ile) ([CO,OH]cc(g_-t)) with the lowest energy alternative, Cs^+(Val) ([CO,OH]cc(t)), having a relative 298 K Gibbs energy of 3.3 kJ/mol or higher. If these two Cs^+(Val) structures were in equilibrium at 298 K, the populations would be 79% cc(g_+) and 21% cc(t) according to MP2 theory. Thus, alternative structures for any of these species probably comprise no more than 21% for any of these species. For Cs^+(hAla), B3LYP and B3LYP-GD3BJ indicate that the cc(t) conformer is the lowest energy structure, whereas MP2 finds a cc(g_-) ground structure. The IR spectra of both structures are considered below

Because the [N,CO]-tt isomer is the assigned structure for lithiated and sodiated Gly,[20, 21] we also checked that this alternative remained relatively high in energy. This is important to check because binding to the amino group puts the ion in a position where it can potentially interact with the side chain. For Cs^+(Gly), the [N,CO]-tt structure lies >11 kJ/mol above the ground structure, Table 2. This relative energy decreases slightly as the side chain length increases, dropping to a low of ~8 kJ/mol for Cs^+(Ile) [N,CO]-$tt_S(g_-t)$. We conclude that consideration of the [N,CO] structures is unlikely to be required, as verified by comparison with experiment below.

Cs^+(Ala) and Cs^+(hAla): Comparison of Experimental and Theoretical Spectra

The IRMPD action spectrum for Cs^+(Ala) has major peaks at 820, 915, 1170 (broad), 1377, and 1730 cm^{-1}, Figure 6. All levels of theory indicate that the ground structure is [CO,OH]-cc, see Table 2. Mode assignments are similar to those for Cs^+(Gly)[CO,OH]-cc. The B3LYP-GD3BJ predicted spectrum (scaled by the same 0.97 factor used for this level of theory for the glycine complex) reproduces the observed spectrum well. If the band at 967 cm^{-1} corresponding to the out-of-plane OH wag were shifted down (by ~50 cm^{-1}) as it did for the CCSD spectrum of Cs^+(Gly), even better reproduction of the experiment would be achieved. In this case, we verified this hypothesis by calculating the spectrum for Cs^+(Ala) at the CCSD/def2-TZVPD level. This spectrum is shown in Figure 6 scaled by 0.94, as for the Cs^+(Gly) system. As hypothesized, the out-of-plane OH wag at 967 cm^{-1} shifts to 912 cm^{-1}. A more minor red-shift in the in-plane OH bend from 1392 to 1376 cm^{-1} is also observed to agree better with experiment.

The IRMPD action spectrum for Cs^+(hAla) has major peaks at 842, 932, 1167, 1368, and 1748 cm^{-1}, see Figure 7. As noted above, theory indicates that the ground structure is [CO,OH]-cc, but the side-chain orientation can be either (t) or (g_-). Mode assignments are similar to those for Cs^+(Gly)[CO,OH]-cc above and the two side-chain orientations yield very similar spectra. The B3LYP-GD3BJ predicted spectra (scaled by the same 0.97 factor used for this level of theory for the glycine complex) reproduces the observed spectrum well. If the bands at 975 and 981 cm^{-1} for the cc(t) conformer or 975 and 979 cm^{-1} for the cc(g_-) conformer, which correspond to the out-of-plane OH wag with different couplings to the side-chain, were shifted down (by ~50 cm^{-1}) as for the CCSD spectrum of Cs^+(Gly), even better reproduction of the experiment would be achieved.

Cs^+(Val), Cs^+(Leu), and Cs^+(Ile): Experimental and Theoretical Spectra

As shown in Figure 1, the spectra for the remaining aliphatic amino acid complexes with Cs^+ are similar to that for Cs^+(Ala), although both Cs^+(Val) and Cs^+(Ile) exhibit three peaks in the 800 – 1000 cm^{-1} region. In agreement with theory, Table 2, this suggests that [CO,OH]-cc conformers continue to dominate the population. The spectrum for Cs^+(Val) is shown in Figure 8 with peaks at 1733, 1386, 1175 (broad), 958 (broad), 893, and 830 cm^{-1}. The predicted spectrum for the [CO,OH]-cc(g_+) structure reproduces the entire spectrum well. Predicted peaks at 829 and

881 cm^{-1} correspond to the NH_2 wagging mode and reproduce the experimental spectrum well. The additional peak at 958 cm^{-1} is predicted at 963 cm^{-1} and has substantial NH_2 wag, out-of-plane OH wag, and side-chain stretching character. If the predicted peak at 984 cm^{-1} (corresponding to nearly pure out-of-plane OH wag) were redshifted, the broadness of the 958 cm^{-1} band would be reproduced even better. Figure 8 also shows the spectrum for the low-lying cc(t) conformer, which has a very similar spectrum as the ground cc(g_+) conformer. The only substantial differences arise in the 800 – 1000 cm^{-1} region. As noted above, if an equilibrium distribution at 298 K of these two conformers were present, the experimental bands in this region would still be reproduced with fidelity. Spectroscopically, it is certainly possible that a small population of the excited cc(t) conformer contributes to the observed spectrum.

Similar comparisons hold for Cs^+(Leu) [CO,OH]-cc(tg_+) and Cs^+(Ile) [CO,OH]-cc(g_-t) when compared to the experimental spectra in Figures 9 and 10. The low-lying cc(g_+g_-) and cc(g_+t) conformers have 298 K equilibrium populations of 14 and 16%, respectively, according to MP2 theory and thus could contribute to the observed spectra. As for the Cs^+(hAla) and Cs^+(Val) complexes, spectra of the different conformations differ only in the 800 – 1000 cm^{-1} range.

CONCLUSION

Overall, IRMPD action spectra of the cesiated complexes of the aliphatic amino acids, Gly, Ala, hAla, Val, Leu, and Ile are similar. In all cases, the results are interpreted using theoretical spectra with the dominant species present corresponding to cesium binding at the carbonyl and hydroxyl oxygen, [CO,OH]-cc. According to calculations, the larger AAs can have small populations of a low-energy conformer in which the side-chain orientation is different, but this leads to only small changes in the spectra. The interesting case of Cs^+(Gly), where previous work had suggested that the [CO]-cc structure is predominantly populated, is explored at additional levels of theory. High-level CCSD(T) results suggest that the potential energy surface connecting the [CO,OH]-cc and [CO]-cc structures does not yield a minimum for [CO]-cc. MP2 calculations reproduce this result with the [CO]-cc structure even less favorable. In contrast, B3LYP does not

yield a minimum for [CO,OH]-cc but only for [CO]-cc. Adding empirical dispersion corrections helps to stabilize the [CO,OH]-cc structure, leading to a double-well potential. The ωB97X-M hybrid functional retains the double-well potential but destabilizes the [CO]-cc structure further. Comparison of the experimental spectrum for Cs^+(Gly) with that predicted by CCSD calculations is consistent with the [CO,OH]-cc structure. Notably, the CCSD calculations red-shift vibrations associated with the out-of-plane OH wagging mode compared with DFT and MP2 calculations. The red shift agrees better with experiment in all systems explored here.

The origins of this challenge to DFT in describing these systems are explored and suggest that electron correlation is critically important and that some common density functionals incorrectly handle the internal hydrogen bonding in these molecules, thereby over-delocalizing the charges on the amino acid ligands. These altered AA charges then appreciably change the electrostatic interaction with—and preferred location of—the cesium cation. These relatively simple systems could serve as key test cases for the development of density functionals, and future experiments that probe the O-H stretching region could further clarify the intramolecular hydrogen-bonding behavior that evidently also indirectly dictates the interaction with the ion.

ASSOCIATED CONTENT

Supporting information

Figure S1 shows a comparison of anharmonic calculations of the [CO,OH]-cc and [CO]-cc structures of Cs^+(Gly) performed at the B3LYP-GD3BJ/6-311+G(d,p) level of theory. Additional figures correspond to the analysis of the inconsistencies between DFT and wave-function based methods for the Cs^+(Gly) complex. This includes additional potential energy scans of the $COCs^+$ bond angle (Figure S2), an energy decomposition analysis as a function of this angle (Figure S3), partial charges on Cs and Gly as a function of this angle (Figure S4), and the effects on the high-frequency vibrations (Figures S5). Figure S6 compares the CCSD spectrum for Cs^+(Gly) [CO,OH]-cc with an experimental spectrum over the range of 1900 – 3400 cm^{-1}.

AUTHOR INFORMATION

Corresponding Author

P. B. Armentrout - Department of Chemistry, University of Utah, 315 S. 1400 E. Rm. 2020, Salt Lake City, Utah 84112, United States; orcid.org/0000-0003-2953-6039;

Email: armentrout@chem.utah.edu

Authors

Ryan P. Steele - Department of Chemistry, University of Utah, 315 S. 1400 E. Rm. 2020, Salt Lake City, Utah 84112, United States; orcid.org/0000-0002-3292-9805

Brandon C. Stevenson - Department of Chemistry, University of Utah, 315 S. 1400 E. Rm. 2020, Salt Lake City, Utah 84112, United States

Roland M. Jones - Department of Chemistry, University of Utah, 315 S. 1400 E. Rm. 2020, Salt Lake City, Utah 84112, United States; Present address: Department of Pathology & Laboratory Medicine, Mail Code H160, Penn State University College of Medicine and Hershey Medical Center, 500 University Drive, Hershey, PA 17033

Jonathan Martens - Radboud University, Institute for Molecules and Materials, FELIX Laboratory, Toernooiveld 7, NL-6525 ED Nijmegen, The Netherlands; orcid.org/0000-0001-9537-4117

Giel Berden - Radboud University, Institute for Molecules and Materials, FELIX Laboratory, Toernooiveld 7, NL-6525 ED Nijmegen, The Netherlands; orcid.org/0000-0003-1500-922X

Jos Oomens - Radboud University, Institute for Molecules and Materials, FELIX Laboratory, Toernooiveld 7, NL-6525 ED Nijmegen, The Netherlands; Van‘t Hoff Institute for Molecular Sciences, University of Amsterdam, Science Park 904, Amsterdam, The Netherlands; orcid.org/0000-0002-2717-1278

ACKNOWLEDGMENTS

This work was financially supported by the National Science Foundation, Grant CHE-2313553 (PBA) and CHE-2102309 (RPS). The authors gratefully acknowledge the *Nederlandse*

Organisatie voor Wetenschappelijk Onderzoek (NWO) for the support of the FELIX Laboratory. A generous grant of computation time from the Center for High Performance Computing at the University of Utah is gratefully appreciated.

References

[1] J.-F. Gal, P.-C. Maria, L. Massi, C. Mayeux, P. Burk, J. Tammiku-Taul, Cesium Cation Affinities and Basicities, Int. J. Mass Spectrom., 267 (2007) 7-23.
[2] S.L. Hood, C.L. Comar, Metabolism of Cesium-137 in Rats and Farm Animals, Arch. Biochem. Biophys., 45 (1953) 423-433.
[3] L.A. Beauge, R.A. Sjodin, Transport of Caesium in Frog Muscle, J. Physiol., 194 (1968) 105-123.
[4] H. Matsuda, H. Matsuura, A. Noma, Triple-Barrel Structure of Inwardly Rectifying K^+ Channels Revealed by Cs^+ and Rb^+ Block in Guinea-Pig Heart Cells, J. Physiol., 413 (1989) 139-157.
[5] A.E. Spruce, N.B. Standen, P.R. Stanfield, Rubidium Ions and the Gating of Delayed Rectifier Potassium Channels of Frog Skeletal Muscle, J. Physiol., 411 (1989) 597-610.
[6] S.R. Relman, A.T. Lambie, B.A. Burrows, A.M. Roy, Cation Accumulation by Muscle Tissue: The Displacement of Potassium by Rubidium and Cesium in the Living Animal, J. Clin. Invest., 36 (1957) 1249-1256.
[7] C.R. Richmond, Retention and Excretion of Radionuclides of the Alkali Metals by Five Mammalian Species, Health Phys., 38 (1980) 1111-1153.
[8] C.K. Yen, T.F. Budinger, Evaluation of Blood-Brain Barrier Permeability Changes in Rhesus Monkeys and Man using ^{82}Rb and Positron Emission Tomography, J. Comp. Assist. Tomog., 5 (1981) 792-799.
[9] P.B. Armentrout, Y. Chen, M.T. Rodgers, Metal Cation Dependence of Interactions with Amino Acids: Bond Energies of Cs^+ to Gly, Pro, Ser, Thr, and Cys, J. Phys. Chem. A, 116 (2012) 3989-3999.
[10] P.B. Armentrout, B. Yang, M.T. Rodgers, Metal Cation Dependence of Interactions with Amino Acids: Bond Energies of Rb^+ and Cs^+ to Met, Phe, Tyr, and Trp, J. Phys. Chem. B, 117 (2013) 3771-3781.
[11] P.B. Armentrout, B. Yang, M.T. Rodgers, Metal Cation Dependence of Interactions with Amino Acids: Bond Dissociation Energies of Rb^+ and Cs^+ to the Acidic Amino Acids and Their Amide Derivatives, J. Phys. Chem. B, 118 (2014) 4300–4314.
[12] P.B. Armentrout, M. Citir, Y. Chen, M.T. Rodgers, Thermochemistry of Alkali Metal Cation Interactions with Histidine: Influence of the Side-Chain, J. Phys. Chem. A, 116 (2012) 11823-11832.
[13] M.K. Drayss, P.B. Armentrout, J. Oomens, M. Schäfer, IR Spectroscopy of Cationized Aliphatic Amino Acids: Stability of Charge-solvated Structure Increases with Metal Cation Size, Int. J. Mass Spectrom., 297 (2010) 18–27.
[14] P.B. Armentrout, M.T. Rodgers, J. Oomens, J.D. Steill, Infrared Multiphoton Dissociation Spectroscopy of Cationized Serine: Effects of Alkali-Metal Cation Size on Gas-Phase Conformation, J. Phys. Chem. A, 112 (2008) 2248-2257.

[15] M.T. Rodgers, P.B. Armentrout, J. Oomens, J.D. Steill, Infrared Multiphoton Dissociation Spectroscopy of Cationized Threonine: Effects of Alkali-Metal Cation Size on Gas-Phase Conformation, J. Phys. Chem. A, 112 (2008) 2258-2267.
[16] M. Citir, E.M.S. Stennett, J. Oomens, J.D. Steill, M.T. Rodgers, P.B. Armentrout, Infrared Multiple Photon Dissociation Spectroscopy of Cationized Cysteine: Effects of Metal Cation Size on Gas-Phase Conformation, Int. J. Mass Spectrom., 297 (2010) 9-17.
[17] D.R. Carl, T.E. Cooper, J. Oomens, J.D. Steill, P.B. Armentrout, Infrared Multiple Photon Dissociation Spectroscopy of Cationized Methionine: Effects of Alkali-Metal Cation Size on Gas-Phase Conformation, Phys. Chem. Chem. Phys., 12 (2010) 3384-3398.
[18] A.L. Heaton, V.N. Bowman, J. Oomens, J.D. Steill, P.B. Armentrout, Infrared Multiple Photon Dissociation Spectroscopy of Cationized Asparagine: Effects of Metal Cation Size on Gas-Phase Conformation, J. Phys. Chem. A, 113 (2009) 5519-5530.
[19] M. Citir, C.S. Hinton, J. Oomens, J.D. Steill, P.B. Armentrout, Infrared Multiple Photon Dissociation Spectroscopy of Cationized Histidine: Effects of Metal Cation Size on Gas-Phase Conformation, J. Phys. Chem. A, 116 (2012) 1532-1541.
[20] P.B. Armentrout, B.C. Stevenson, M. Ghiassee, G.C. Boles, G. Berden, J. Oomens, Infrared Multiple-photon Dissociation Spectroscopy of Cationized Glycine: Effects of Alkali Metal Cation Size on Gas-phase Conformation, Phys. Chem. Chem. Phys., 24 (2022) 22950-22959.
[21] C. Kapota, J. Lemaire, P. Maitre, G. Ohanessian, Vibrational Signature of Charge Solvation vs Salt Bridge Isomers of Sodiated Amino Acids in the Gas Phase, J. Am. Chem. Soc., 126 (2004) 1836-1842.
[22] J.T. O'Brien, J.S. Prell, J.D. Steill, J. Oomens, E.R. Williams, Interactions of Mono- and Divalent Metal Ions with Aspartic and Glutamic Acid Investigated with IR Photodissociation Spectroscopy and Theory, J. Phys. Chem. A, 112 (2008) 10823-10830.
[23] R.M. Jones, T. Nilsson, S. Walker, P.B. Armentrout, Potassium Binding Interactions with Aliphatic Amino Acids: Thermodynamic and Entropic Effects Analyzed via a Guided Ion Beam and Computational Study, J. Am. Soc. Mass Spectrom., 33 (2022) 1427-1442.
[24] D. Oepts, A.F.G. van der Meer, P.W. van Amersfoort, The Free-Electron-Laser User Facility FELIX, Infrared Phys. Technol., 36 (1995) 297-308.
[25] J. Martens, G. Berden, C.R. Gebhardt, J. Oomens, Infrared ion spectroscopy in a modified quadrupole ion trap mass spectrometer at the FELIX free electron laser laboratory, Rev. Sci. Instrum., 87 (2016) 103108.
[26] G. Berden, M. Derksen, K.J. Houthuijs, J. Martens, J. Oomens, An Automatic Variable Laser Attenuator for IRMPD Spectroscopy and Analysis of Power-dependence in Fragmentation Spectra, Int. J. Mass Spectrom., 443 (2019) 1-8.
[27] J. Lemaire, P. Boissel, M. Heninger, G. Mauclaire, G. Bellec, H. Mestdagh, S. Le Caer, J. Ortega, F. Glotin, P. Maître, Gas Phase Infrared Spectroscopy of Selectively Prepared Ions, Phys. Rev. Lett., 89 (2002) 273002.
[28] M.J. Frisch, G.W. Trucks, H.B. Schlegel, G.E. Scuseria, M.A. Robb, J.R. Cheeseman, G. Scalmani, V. Barone, G.A. Petersson, H. Nakatsuji, X. Li, M. Caricato, A.V. Marenich, J. Bloino, B.G. Janesko, R. Gomperts, B. Mennucci, H.P. Hratchian, J.V. Ortiz, A.F. Izmaylov, J.L. Sonnenberg, D. Williams-Young, F. Ding, F. Lipparini, F. Egidi, J. Goings, B. Peng, A. Petrone, T. Henderson, D. Ranasinghe, V.G. Zakrzewski, J. Gao, N. Rega, G. Zheng, W. Liang, M. Hada, M. Ehara, K. Toyota, R. Fukuda, J. Hasegawa, M. Ishida, T. Nakajima, Y. Honda, O. Kitao, H. Nakai, T. Vreven, K. Throssell, J. J. A. Montgomery, J.E. Peralta, F. Ogliaro, M.J. Bearpark, J.J. Heyd, E.N. Brothers, K.N. Kudin, V.N. Staroverov, T.A. Keith, R. Kobayashi, J. Normand, K.

Raghavachari, A.P. Rendell, J.C. Burant, S.S. Iyengar, J. Tomasi, M. Cossi, J.M. Millam, M. Klene, C. Adamo, R. Cammi, J.W. Ochterski, R.L. Martin, K. Morokuma, O. Farkas, J.B. Foresman, D.J. Fox, Gaussian 16, Revision A.03, in, Gaussian, Inc., Wallingford CT, 2016.
[29] A.D. Becke, Density-functional Exchange Energy Approximation with Correct Asymptotic Behavior, Phys. Rev. A, 38 (1988) 3098-3100.
[30] C. Lee, W. Yang, R.G. Parr, Development of the Colle-Salvetti Correlation-Energy Formula into a Functional of the Electron Density, Phys. Rev. B, 37 (1988) 785-789.
[31] R. Ditchfield, W.J. Hehre, J.A. Pople, Self-Consistent Molecular-Orbital Methods. IX. An Extended Gaussian-Type Basis for Molecular-Orbital Studies of Organic Molecules, J. Chem. Phys., 54 (1971) 724-728.
[32] S. Grimme, S. Ehrlich, L. Goerigk, Effect of the Damping Function in Dispersion Corrected Density Functional Theory, J. Comput. Chem., 32 (2011) 1456-1465.
[33] S. Grimme, J. Antony, S. Ehrlich, H. Krieg, A Consistent and Accurate Ab Initio Parametrization of Density Functional Dispersion Correction (DFT-D) for the 94 Elements H-Pu, J. Chem. Phys., 132 (2010) 154104-154119.
[34] C. Möller, M.S. Plesset, Note on an Approximation Treatment for Many-Electron Systems, Phys. Rev., 46 (1934) 618-622.
[35] B.P. Pritchard, D. Altarawy, B. Didier, T.D. Gibson, T.L. Windus, A New Basis Set Exchange: An Open, Up-to-date Resource for the Molecular Sciences Community, J. Chem. Inf. Model., 59 (2019) 4814-4820.
[36] J.B. Foresman, A.E. Frisch, Exploring Chemistry with Electronic Structure Methods, 2nd ed., Gaussian, Inc., Pittsburgh, PA, 1996.
[37] C.W. Bauschlicher, H. Partridge, A modification of the Gaussian-2 approach using density functional theory, J. Chem. Phys., 103 (1995) 1788-1791.
[38] S.A. Kucharski, R.J. Bartlett, The Coupled-cluster Single, Double, Triple, and Quadruple Excitation Method, J. Chem. Phys., 97 (1992) 4282-4288.
[39] M.J.O. Deegan, P.J. Knowles, Perturbative corrections to account for triple excitations in closed and open shell coupled cluster theories, Chem. Phys. Lett., 227 (1994) 321-326.
[40] J. Sun, A. Ruzsinszky, J.P. Perdew, Strongly Constrained and Appropriately Normed Semilocal Density Functional, Phys. Rev. Lett., 115 (2015) 036402.
[41] N. Mardirossian, M. Head-Gordon, ωB97M-V: A combinatorially optimized, range-separated hybrid, meta-GGA density functional with VV10 nonlocal correlation, J. Chem. Phys., 144 (2016) 214110.
[42] J.G. Hill, K.A. Peterson, Gaussian basis sets for use in correlated molecular calculations. XI. Pseudopotential-based and all-electron relativistic basis sets for alkali metal (K–Fr) and alkaline earth (Ca–Ra) elements, J. Chem. Phys., 147 (2017).
[43] I.S. Lim, P. Schwerdtfeger, B. Metz, H. Stoll, All-electron and relativistic pseudopotential studies for the group 1 element polarizabilities from K to element 119, J. Chem. Phys., 122 (2005).
[44] T.H. Dunning, Gaussian basis sets for use in correlated molecular calculations. I. The atoms boron through neon and hydrogen, J. Chem. Phys., 90 (1989) 1007-1023.
[45] M.U. Munshi, G. Berden, J. Martens, J. Oomens, Gas-phase vibrational spectroscopy of triphenylamine: the effect of charge on structure and spectra, Phys. Chem. Chem. Phys., 19 (2017) 19881-19889.
[46] R.E. van Outersterp, J. Martens, A. Peremans, L. Lamard, F. Cuyckens, J. Oomens, G. Berden, Evaluation of table-top lasers for routine infrared ion spectroscopy in the analytical laboratory, Analyst, 146 (2021) 7218-7229.

[47] N.C. Polfer, J. Oomens, R.C. Dunbar, IRMPD Spectroscopy of Metal-Ion/Tryptophan Complexes, Phys. Chem. Chem. Phys., 8 (2006) 2744-2751.
[48] R.C. Dunbar, N.C. Polfer, J. Oomens, Gas-phase zwitterion stabilization by a metal dication, J. Am. Chem. Soc., 129 (2007) 14562-14563.
[49] M.W. Forbes, M.F. Bush, N.C. Polfer, J. Oomens, R.C. Dunbar, E.R. Williams, R.A. Jockusch, Infrared Spectroscopy of Arginine Cation Complexes: Direct Observation of Gas-Phase Zwitterions, J. Phys. Chem. A, 111 (2007) 11759-11770.
[50] M.F. Bush, M.W. Forbes, R.A. Jockusch, J. Oomens, N.C. Polfer, R.J. Saykally, E.R. Williams, Infrared Spectroscopy of Cationized Lysine and ε-N-methyllysine in the Gas Phase: Effects of Alkali-Metal Ion Size and Proton Affinity on Zwitterion Stability, J. Phys. Chem. A, 111 (2007) 7753-7760.
[51] M.F. Bush, J.T. O'Brien, J.S. Prell, R.J. Saykally, E.R. Williams, Infrared Spectroscopy of Cationized Arginine in the Gas Phase: Direct Evidence for the Transition from Nonzwitterionic to Zwitterionic Structure, J. Am. Chem. Soc., 129 (2007) 1612-1622.
[52] M.K. Drayss, D. Blunk, J. Oomens, M. Schäfer, Infrared Multiple Photon Dissociation Spectroscopy of Potassiated Proline, J. Phys Chem. A, 112 (2008) 11972-11974.
[53] M.F. Bush, J. Oomens, R.J. Saykally, E.R. Williams, Effects of Alkaline Earth Metal Ion Complexation on Amino Acid Zwitterion Stability: Results from Infrared Action Spectroscopy, J. Am. Chem. Soc., 130 (2008) 6463-6471.
[54] M.F. Bush, J. Oomens, R.J. Saykally, E.R. Williams, Alkali Metal Ion Binding to Glutamine and Glutamine Derivatives Investigated by Infrared Action Spectroscopy and Theory, J. Phys. Chem. A, 112 (2008) 8578-8584.
[55] M.F. Bush, J. Oomens, E.R. Williams, Proton Affinity and Zwitterion Stability: New Results from Infrared Spectroscopy and Theory of Cationized Lysine and Analogues in the Gas Phase, J. Phys. Chem. A, 113 (2009) 431-438.
[56] R.C. Dunbar, J.D. Steill, J. Oomens, Cationized phenylalanine conformations characterized by IRMPD and computation for singly and doubly charged ions, Phys. Chem. Chem. Phys., 12 (2010) 13383-13393.
[57] P.B. Armentrout, G.C. Boles, M. Ghiassee, G. Berden, J. Oomens, Infrared Multiple-Photon Dissociation Spectra of Sodiated Complexes of the Aliphatic Amino Acids, J. Phys. Chem. A, 125 (2021) 6348-6355.
[58] R.Z. Khaliullin, E.A. Cobar, R.C. Lochan, A.T. Bell, M. Head-Gordon, Unravelling the Origin of Intermolecular Interactions Using Absolutely Localized Molecular Orbitals, J. Phys. Chem. A, 111 (2007) 8753-8765.
[59] J.K. Martens, J. Grzetic, G. Berden, J. Oomens, Gas-phase conformations of small polyprolines and their fragment ions by IRMPD spectroscopy, Int. J. Mass Spectrom., 377 (2015) 179-187.
[60] J.A. Fournier, C.T. Wolke, M.A. Johnson, T.T. Odbadrakh, K.D. Jordan, S.M. Kathmann, S.S. Xantheas, Snapshots of Proton Accommodation at a Microscopic Water Surface: Understanding the Vibrational Spectral Signatures of the Charge Defect in Cryogenically Cooled H+(H2O)n=2–28 Clusters, J. Phys. Chem. A, 119 (2015) 9425-9440.

Table 1. Computed ChElPG atomic charges in Cs^+(Gly) (MP2-optimized structure) and isolated Gly (optimized for each method), using the cc-pwCVTZ-PP basis set.

	Cs^+(Gly)			Gly			
Method	Cs	O_{OH}	O_{CO}	O_{OH}	H_{OH}	N	O_{CO}
HF	0.923	-0.583	-0.654	-0.545	0.355	-0.894	-0.618
B3LYP	0.925	-0.518	-0.589	-0.494	0.317	-0.792	-0.559
ωB97M-V	0.937	-0.525	-0.584	-0.496	0.324	-0.805	-0.557
MP2	0.916	-0.540	-0.565	-0.500	0.328	-0.811	-0.527

Table 2. Relative 0 K enthalpies (298 K Gibbs energies) in kJ/mol of Cs^+(AA) structures.[a]

AA	Structure	B3LYP		B3LYP-GD3BJ		MP2(full)	
Gly	[CO,OH]cc	1.07	(1.60)	0.36	(0.89)	**0.00**	(**0.00**)
	[CO]cc	**0.00**	(**0.00**)	**0.00**	(**0.00**)	2.48	(1.95)
	[N,CO]tt	11.43	(15.39)	7.58	(11.55)	9.02	(12.46)
Ala	[COOH]cc	**0.00**	(**0.00**)	**0.00**	(**0.00**)	**0.00**	(**0.00**)
	[N,CO]tt$_S$	11.30	(14.22)	6.79	(9.71)	8.03	(10.95)
	[N,CO]tt$_A$	13.10	(15.61)	9.62	(12.14)	11.34	(13.86)
hAla	[CO,OH]cc(t)	**0.00**	(**0.00**)	**0.00**	(**0.00**)	0.43	(0.68)
	[CO,OH]cc(g$_-$)	3.01	(2.75)	1.13	(0.88)	**0.00**	(**0.00**)
	[CO,OH]cc(g$_+$)	5.44	(5.69)	4.60	(4.85)	3.98	(4.48)
	[N,CO]tt$_S$(t)	12.53	(14.81)	7.45	(9.73)	8.78	(11.11)
	[N,CO]tt$_S$(g$_-$)	15.45	(19.26)	6.32	(10.13)	5.43	(9.29)
Val	[CO,OH]cc(g$_+$)	**0.00**	(**0.00**)	**0.00**	(**0.00**)	**0.00**	(**0.00**)
	[CO,OH]cc(t)	5.26	(5.59)	4.19	(4.52)	2.99	(3.31)
	[CO,OH]cc(g$_-$)	7.66	(6.91)	8.08	(7.33)	7.70	(6.95)
	[N,CO]tt$_A$(g$_+$)	13.08	(14.93)	9.18	(11.03)	10.32	(12.17)
	[N,CO]tt$_S$(g$_+$)	13.88	(16.92)	6.00	(9.04)	5.47	(8.51)
Leu	[CO,OH]cc(tg$_+$)	**0.00**	(**0.00**)	**0.00**	(**0.00**)	**0.00**	(**0.00**)
	[CO,OH]cc(g$_+$g$_-$)	6.50	(7.63)	5.23	(6.36)	3.44	(4.57)
	[N,CO]tt$_S$(tg$_+$)	12.50	(15.38)	6.79	(9.67)	7.06	(9.95)
	[N,CO]tt$_S$(tg$_-$)	18.23	(21.61)	12.37	(15.75)	14.20	(17.57)
	[CO,OH]cc(g$_+$t)	21.80	(23.90)	17.15	(19.25)	15.31	(17.41)
Ile	[CO,OH]cc(g$_-$t)	**0.00**	(**0.00**)	**0.00**	(**0.00**)	**0.00**	(**0.00**)
	[CO,OH]cc(g$_+$t)	5.21	(5.68)	4.52	(4.99)	3.63	(4.10)
	[CO,OH]cc(tt)	8.31	(8.09)	8.96	(8.74)	9.00	(8.78)
	[CO,OH]cc(g$_-$g$_-$)	10.37	(11.51)	7.52	(8.67)	7.23	(8.38)
	[N,CO]tt$_A$(g$_-$t)	13.08	(15.17)	9.20	(11.28)	10.31	(12.40)
	[N,CO]tt$_S$(g$_-$t)	14.05	(17.65)	5.52	(9.11)	4.46	(8.06)

[a] Single point energies calculated at the level shown, Level/def2-TZVPPD//Level/def2-TZVP, with zero point and thermal corrections determined at the B3LYP-GD3BJ/def2-TZVP level (scaled by 0.989).

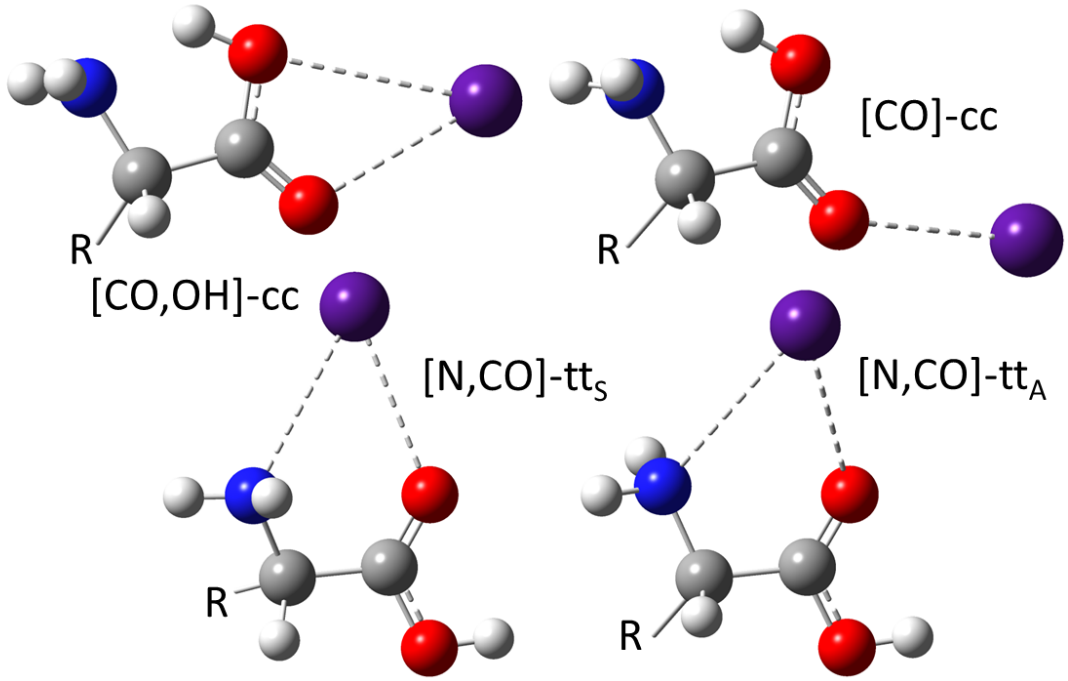

Figure 1. Possible low-energy structures for Cs^+(AA) complexes. White – H, grey – C, blue – N, red – O, and purple – Cs. Dashed lines show metal-ligand interactions.

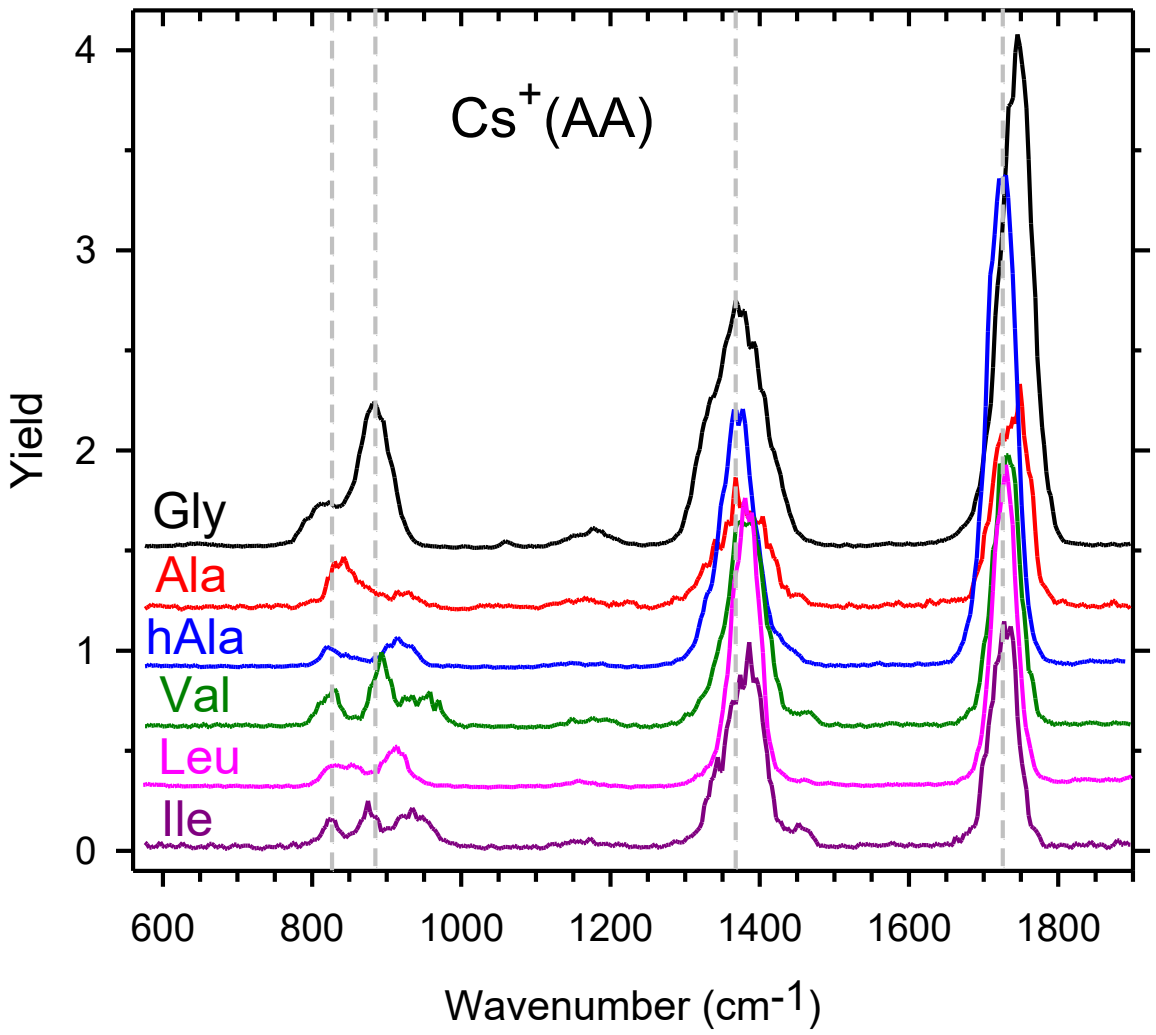

Figure 2. Comparison of the IRMPD spectra of six Cs^+(AA) complexes with baselines offset for clarity. Vertical lines are guides to the eye.

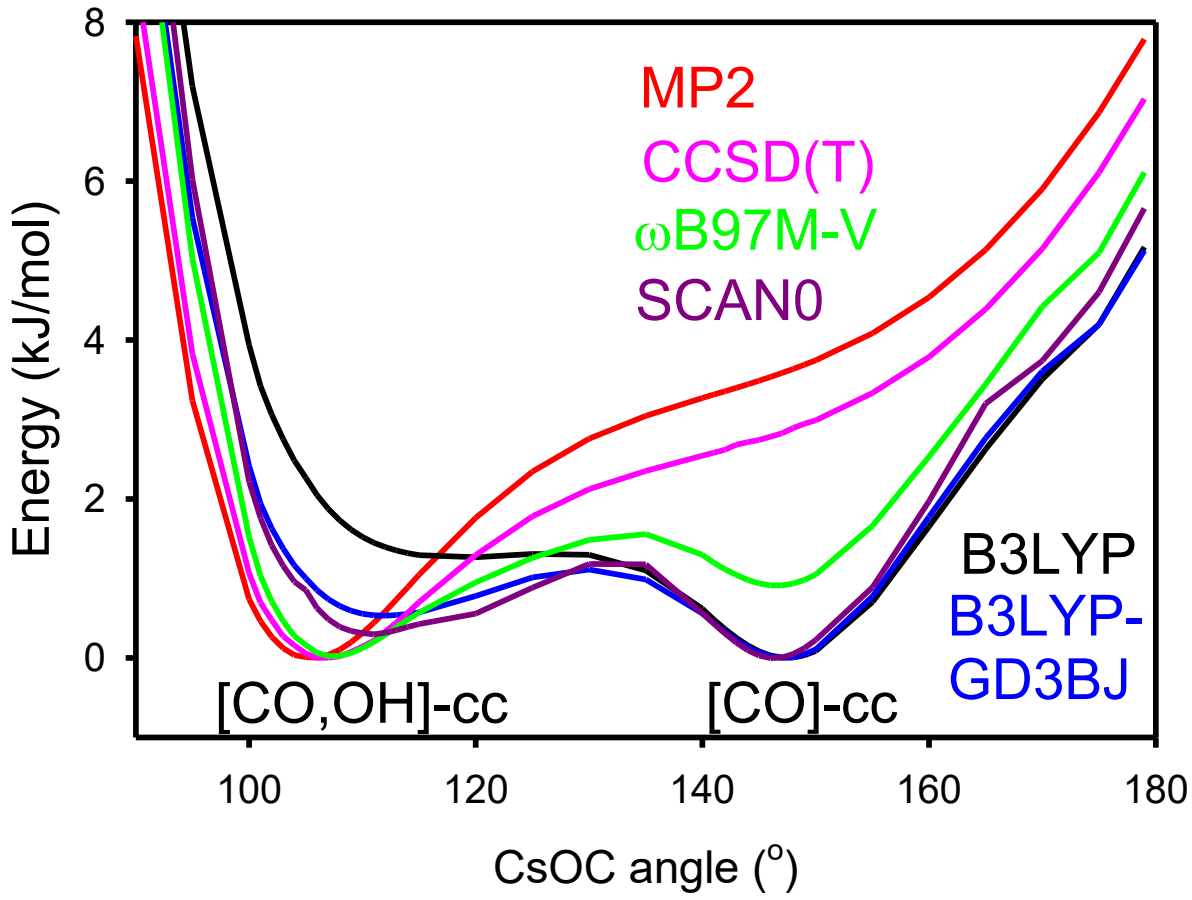

Figure 3. Relaxed potential energy surface scans of the $CsO_{CO}C$ bond angle in Cs^{+}(Gly) calculated at the B3LYP, B3LYP-GD3BJ, SCAN0, ωB97M-V, CCSD(T), and MP2 levels of theory.

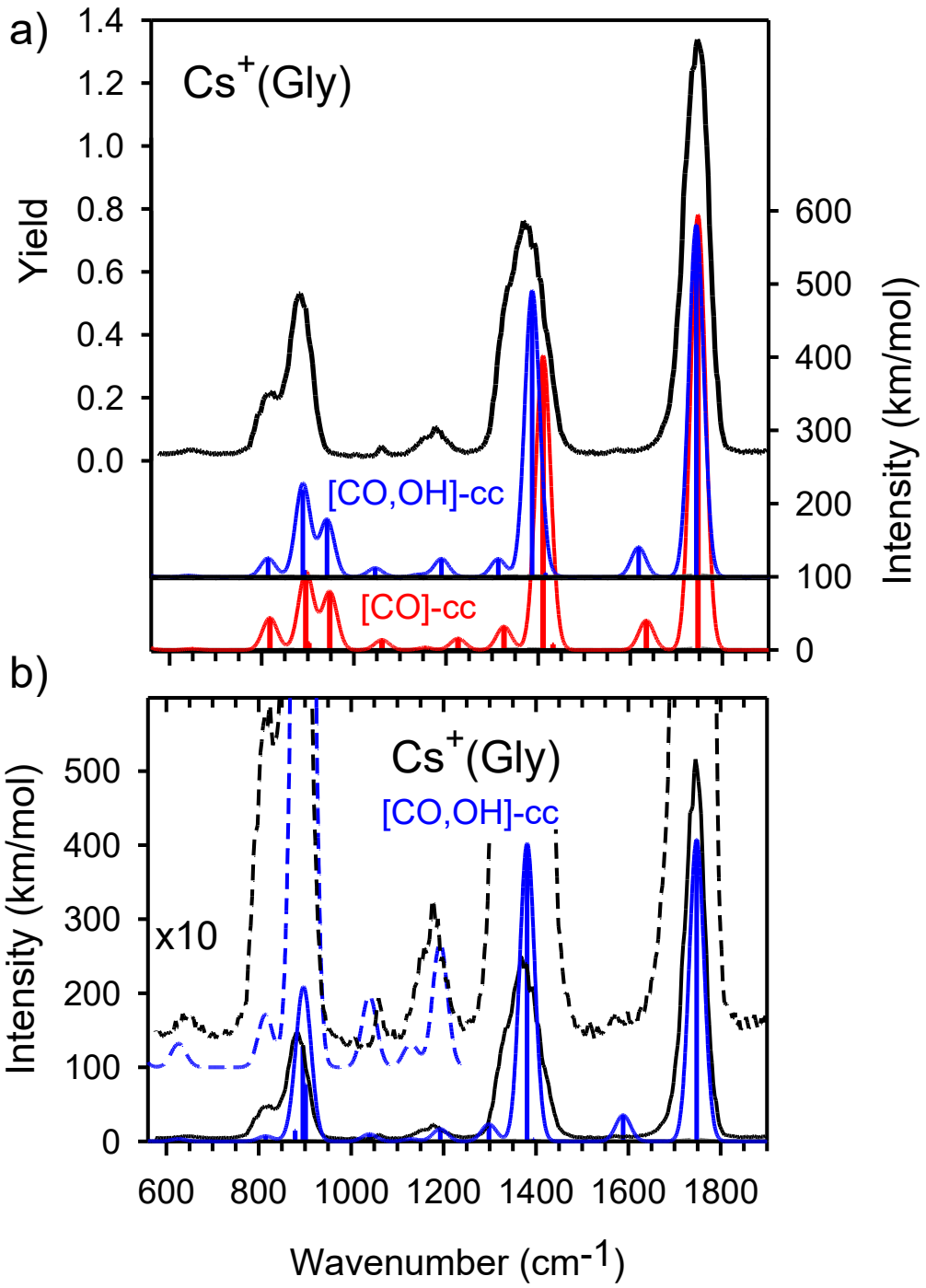

Figure 4. Part a. Comparison of the Cs^+(Gly) experimental IRMPD action spectrum (black) with IR spectra calculated at the B3LYP-GD3BJ/def2-TZVP level of theory for the [CO,OH]-cc (blue, scaled by 0.97) and [CO]-cc (red, scaled by 0.98) conformer. Part b. Comparison of the Cs^+(Gly) experimental IRMPD action spectrum (black) with IR spectra calculated at the CCSD/cc-pwCVTZ-PP level of theory for the [CO,OH]-cc (blue, scaled by 0.94) conformer.

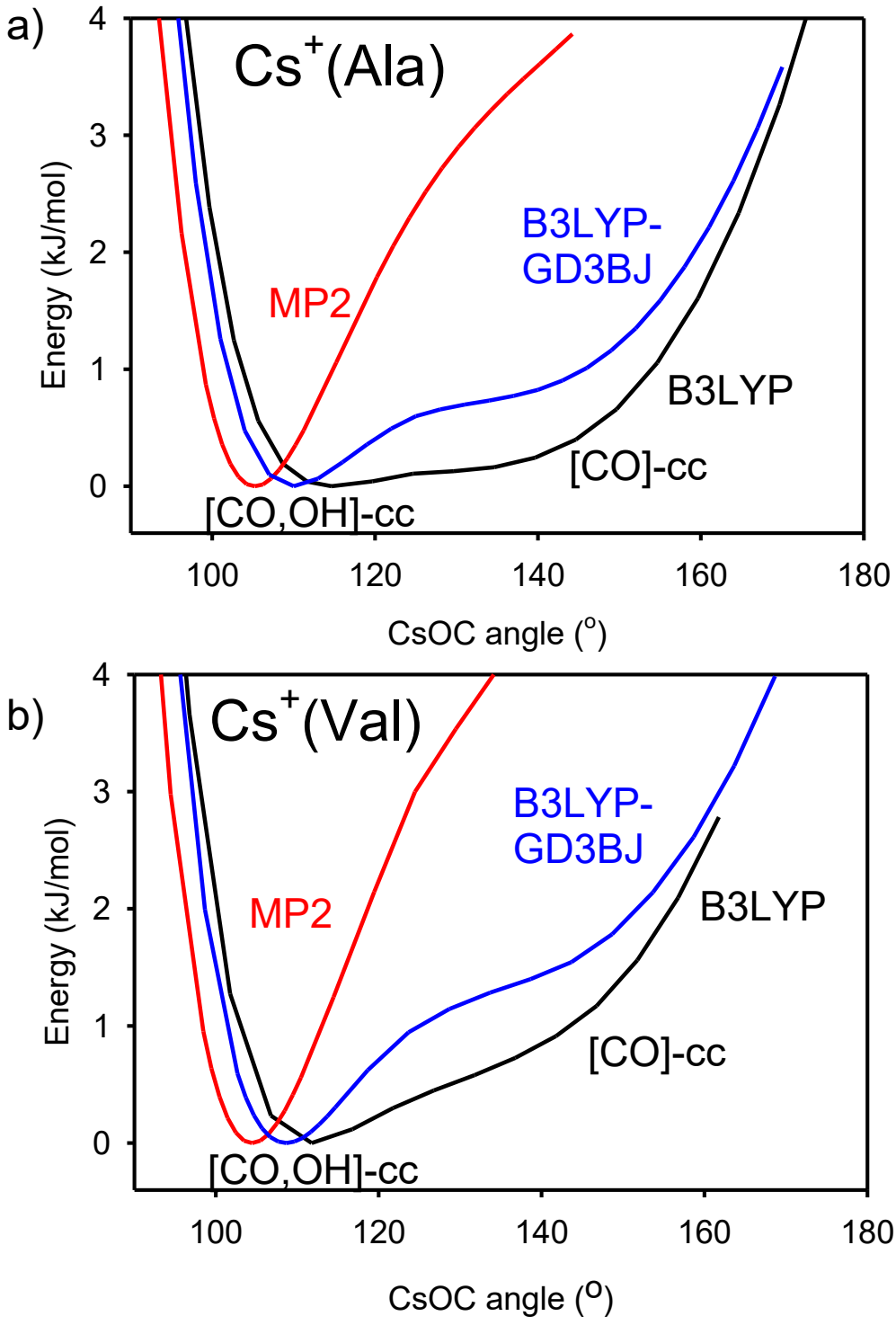

Figure 5. Relaxed potential energy surface scans of the CsOC bond angle in Cs^+(Ala) (part a) and Cs^+(Val) (part b) calculated at the B3LYP, B3LYP-GD3BJ, and MP2(full) levels of theory using a def2-TZVP basis set.

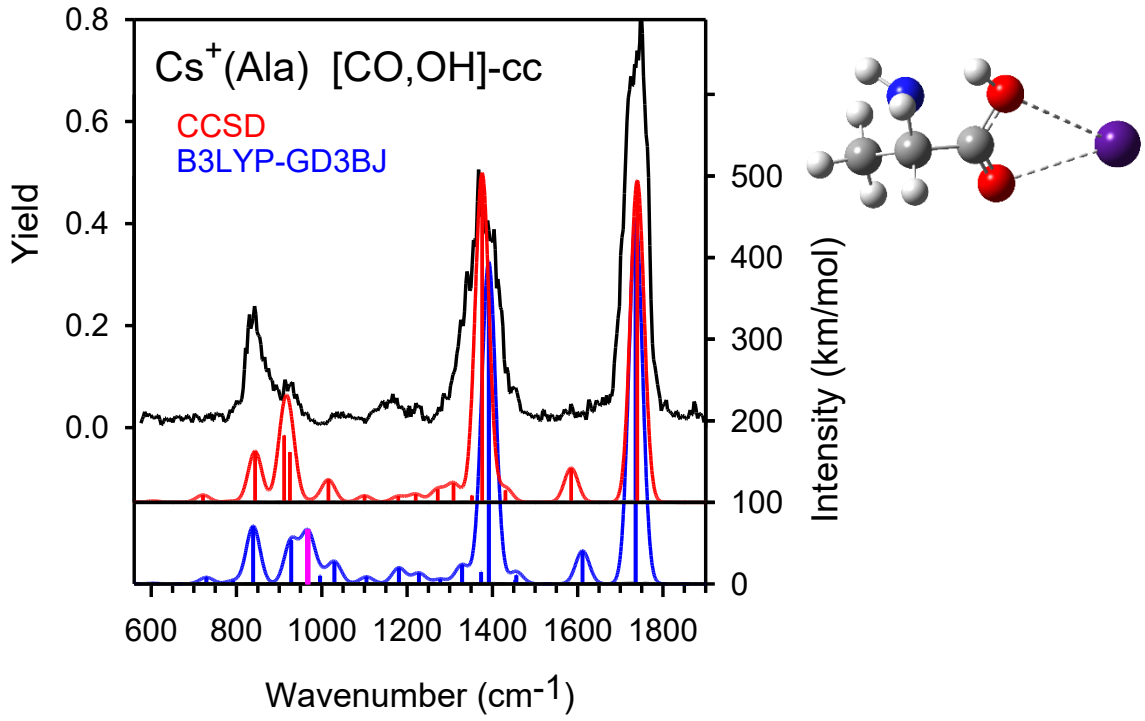

Figure 6. Comparison of the Cs^+(Ala) experimental IRMPD action spectrum (black) with IR spectra calculated at the CCSD/def2-TZVP (red, scaled by 0.94) and B3LYP-GD3BJ/def2-TZVP (blue, scaled by 0.97) levels of theory for the [CO,OH]-cc conformer. The pink line shows the vibration that shifts to lower frequency compared to that calculated at a CCSD level.

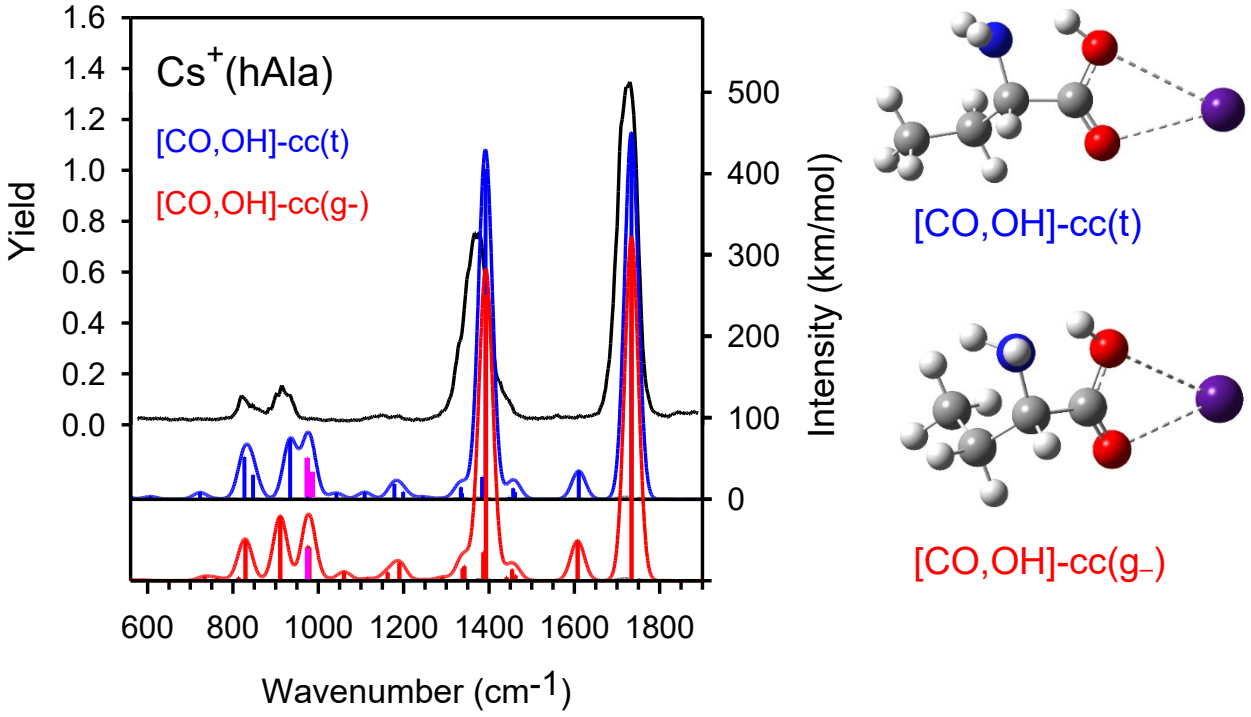

Figure 7. Comparison of the Cs^+(hAla) experimental IRMPD action spectrum (black) with IR spectra calculated at the B3LYP-GD3BJ/def2-TZVP level of theory for the [CO,OH]-cc(t) (blue) and cc(g-) (red) conformer (structures shown to right) scaled by 0.97. The pink lines show the vibration expected to shift to lower energies when calculated at a CCSD level.

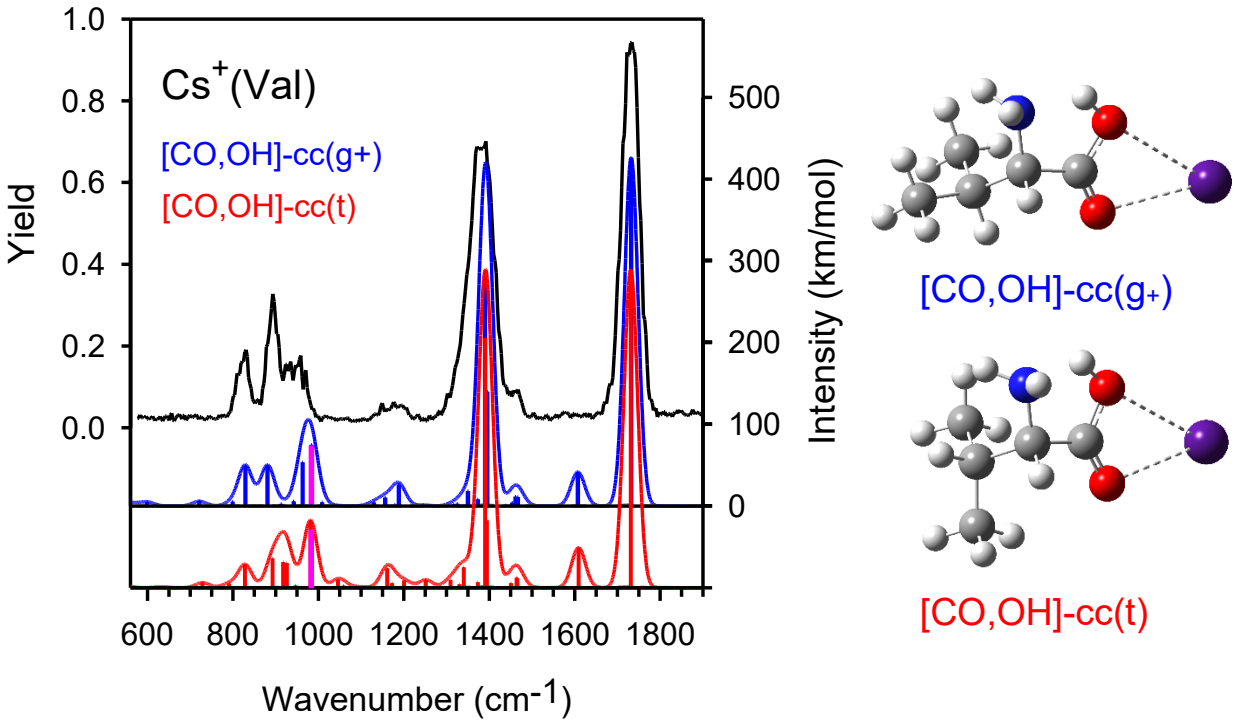

Figure 8. Comparison of the Cs^+(Val) experimental IRMPD action spectrum (black) with IR spectra calculated at the B3LYP-GD3BJ/def2-TZVP level of theory for the [CO,OH]-cc(g_+) (blue) conformer (structure shown to right) scaled by 0.97. The pink line shows the vibration expected to shift to lower energies when calculated at a CCSD level.

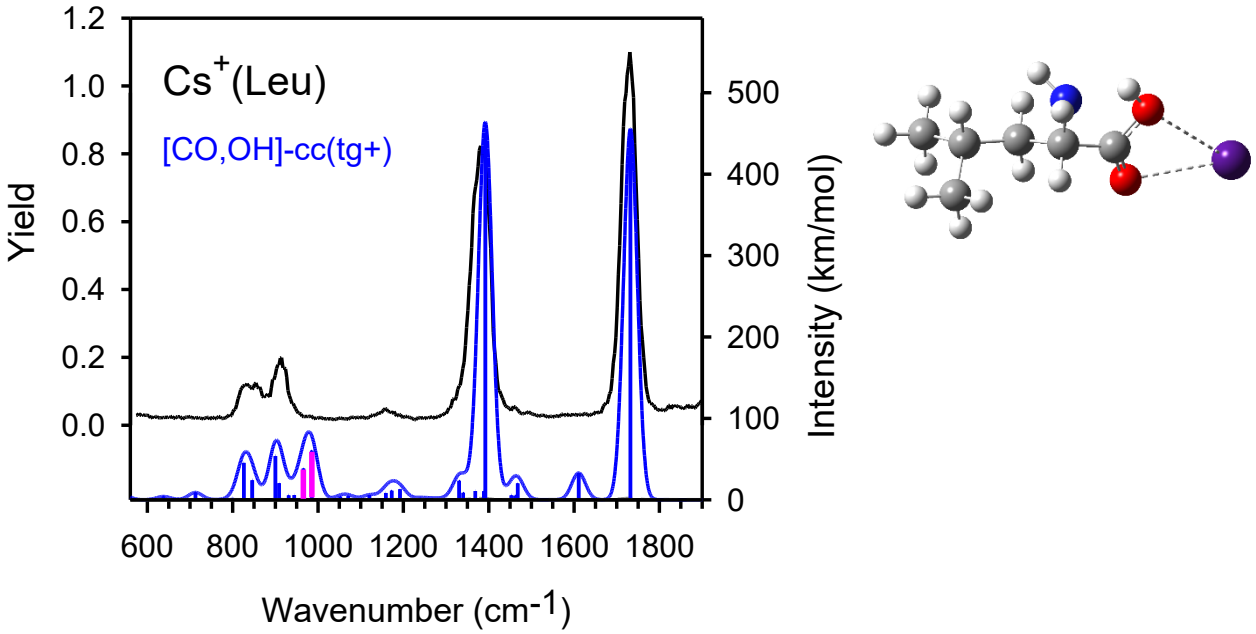

Figure 9. Comparison of the Cs^+(Leu) experimental IRMPD action spectrum (black) with IR spectra calculated at the B3LYP-GD3BJ/def2-TZVP level of theory for the [CO,OH]-cc(tg_+) (blue) conformer (structure shown to right) scaled by 0.97. The pink line shows the vibration expected to shift to lower energies when calculated at a CCSD level.

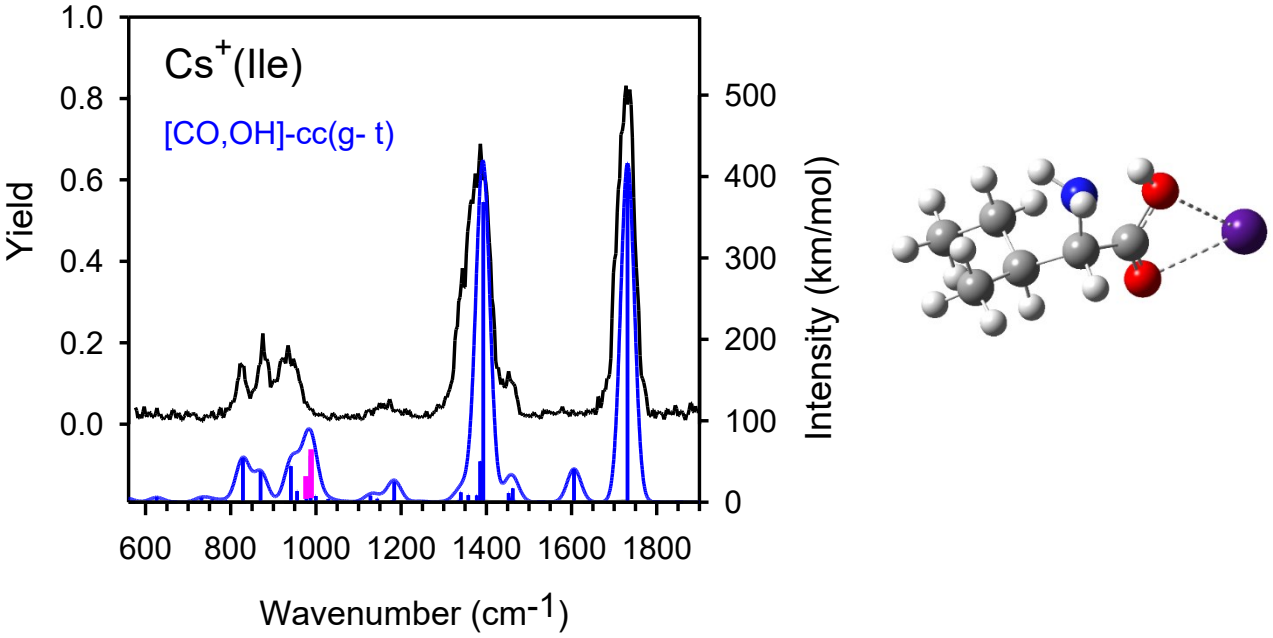

Figure 10. Comparison of the Cs^+(Ile) experimental IRMPD action spectrum (black) with IR spectra calculated at the B3LYP-GD3BJ/def2-TZVP level of theory for the [CO,OH]-cc(g_t) (blue) conformer (structure shown to right) scaled by 0.97. The pink line shows the vibration expected to shift to lower energies when calculated at a CCSD level.

TOC Graphic